Fermilab

Kinematically-enhanced interpolating operators for boosted hadrons

FERMILAB-PUB-24-0968-T

arXiv:2501.00729

FERMILAB-PUB-24-0968-T

Kinematically-enhanced interpolating operators for boosted hadrons

Rui Zhang,[1,*] Anthony V. Grebe,[2] Daniel C. Hackett,[2] Michael L. Wagman,[2] and Yong Zhao[1]

[1] *Physics Division, Argonne National Laboratory, Lemont, IL 60439, USA*
[2] *Fermi National Accelerator Laboratory, Batavia, IL 60510, USA*

We propose to use interpolating operators for lattice quantum chromodyanmics (QCD) calculations of highly-boosted pions and nucleons with kinematically-enhanced ground-state overlap factors at large momentum. Because this kinematic enhancement applies to the signal but not the variance of the correlation function, these interpolating operators can achieve better signal-to-noise ratios at large momentum. We perform proof-of-principle calculations with boosted pions and nucleons using close-to-physical and larger quark masses to explore the utility of our proposal. Results for effective energies and matrix elements, as well as Lanczos ground-state energy estimators, are consistent with theoretical expectations for signal-to-noise improvement at large momenta.

Boosted hadrons are commonly required in studies of hadron structure and interactions including calculations of form factors at large Q^2 [1–4] and partonic physics using near-lightcone approximations [5–15]. Recent lattice quantum chromodynamics (QCD) calculations have employed pions with boosts of 2.4 GeV [16], as well as kaons and baryons with boosts of 3 GeV [4, 17, 18]. However, the signal-to-noise ratios (SNRs) for hadronic observables decrease rapidly when the hadron state is boosted to large momentum, limiting the ability of lattice QCD calculations to reliably extract ground-state signals. Techniques to improve the precision and reliability of lattice QCD calculations including highly boosted hadron states are thus extremely desirable.

Attempts to design interpolating operators (interpolators) achieving better signals for highly boosted hadron states have primarily focused on the spatial structure of the quark fields. Early attempts included anisotropic spatial smearing resembling a "plate"-like picture of hadrons in a Minkowski boosted frame [19, 20], but these operators did not show significant SNR improvement and seemed to worsen excited-state effects. Significant progress was achieved through the proposal of momentum smearing quark propagators [21], which enhances both the SNR and overlap of standard hadron interpolators with boosted states. In this approach, the fermion fields are smeared with a phase factor to simulate a wave packet carrying specific momentum on the lattice. Momentum smearing can lead to order-of-magnitude improvement in the SNR for large boosts, and its use is now standard in lattice QCD calculations of highly boosted hadrons [14, 15].

Designing optimal spinor structures for highly boosted hadron interpolators has received less attention. Standard interpolators acting on the vacuum create quark (antiquark) Fock states with the quantum numbers and symmetry properties of rest-frame hadrons and then multiply these states by a momentum phase factor. Physically, highly boosted hadrons can be described by a lightcone field theory picture where there are an infinite set of Fock states. The leading lightcone Fock states for highly boosted pions and nucleons are constructed from the "plus" component of the quark spinors [22, 23], while the overlap with standard interpolators includes a subleading lightcone wave function.

In this *Letter*, we construct interpolators associated with the leading lightcone Fock states for pions and nucleons. We study the Parisi-Lepage scaling [24, 25] of correlation functions (correlators) built from these interpolators and show that their SNR is enhanced for large boosts P by a kinematic factor proportional to P^2. Proof-of-principle numerical calculations corroborate these theoretical expectations. We find that although excited-state effects are larger for these new interpolators than standard ones, the differences in excited-state effects become smaller for larger boosts. To quantify SNR improvements in ground-state energy determinations, we use the Lanczos framework for correlator analysis introduced in Refs. [26–28], which provides ground-state energy estimators with asymptotically constant SNR for boosted hadrons. For the setup considered here, kinematically-enhanced interpolators lead to $\mathcal{O}(100)$-fold SNR improvement for pions with boosts of $P > 2$ GeV and $\mathcal{O}(10)$-fold SNR improvement for nucleons with boosts of $P > 3$ GeV. Analogous SNR improvements are seen in three-point correlators, suggesting that these new interpolators can significantly improve the precision of lattice QCD studies of parton physics.

A variety of other applications can also be imagined for highly boosted pion interpolators; for example, studies of $K \to \pi\pi$ decays sensitive to beyond-the-Standard-Model CP violation involve $\pi\pi$ states where each pion has energy of the order of the kaon mass [29–33] and $\mathcal{O}(10)$-fold SNR gains can be expected. Even larger gains could be achieved in applications to B meson decays or studies of relatively high-energy $\pi\pi$ scattering.

Kinematic enhancement: theory — In the lightcone limit, a Dirac spinor can be decomposed into $\psi = \psi_+ + \psi_-$ with $\psi_\pm = \frac{1}{\sqrt{2}}\gamma_\mp\gamma_\pm\psi$, in which the "plus" component ψ_+ dominates the dynamics [22, 23]. Orienting the hadron momentum as $\vec{P} = |\vec{P}|\hat{e}_z$, the lightcone gamma matrices are $\gamma_\pm \equiv \frac{1}{\sqrt{2}}(\gamma_t \pm i\gamma_z)$, where $\gamma_t \equiv \gamma_4$

*Electronic address: ruizhang@anl.gov

and $\gamma_z \equiv \gamma_3$ are Euclidean gamma matrices satisfying $\gamma_\mu^\dagger = \gamma_\mu$ and $\{\gamma_\mu, \gamma_\nu\} = 2\delta_{\mu\nu}$; Minkowski versions are related by $\gamma_4 = \gamma_0^M$ and $i\gamma_i = \gamma_i^M$. Thus quark bilinears constructed with only ψ_+ components describe the leading Fock states of mesons with mass M in the expansion of $M/(E+P_z)$. For pseudoscalar mesons like the pion, the leading contribution is $u_+^\dagger \gamma_5 d_+ = \sqrt{2}\bar{u}\gamma_+\gamma_5 d$. On the other hand, the traditional pseudoscalar operator $(\bar{u}\gamma_5 d) = (u_+^\dagger \gamma_t\gamma_5 d_- + u_-^\dagger \gamma_t\gamma_5 d_+)/2$ is associated with subleading Fock states. These lightcone physics considerations suggest that $(\bar{u}\gamma_\mu\gamma_5 d)$ operators should have better overlap with highly boosted pion ground states.

Axial-vector pion operators $(\bar{u}\gamma_\mu\gamma_5 d)$ transform differently from standard pseudoscalar pion operators $(\bar{u}\gamma_5 d)$ under rotations and only $(\bar{u}\gamma_t\gamma_5 d)$ has non-zero overlap with the pion ground state in the rest frame. Conversely, the axial-vector current $(\bar{u}\gamma_z\gamma_5 d)$ has the same quantum numbers as an axial-vector meson and thus can be used to study the spectrum of mesons with axial-vector quantum numbers at $P_z = 0$, including the $a_1(1260)$ resonance. However, rotational symmetry is broken for hadron states with non-zero $\vec{P}$, which allows $(\bar{u}\gamma_z\gamma_5 d)$ to overlap with the same states as pseudoscalar pion operators. This effect is familiar in the context of calculating the pion decay constant using the cross-correlation of $(\bar{u}\gamma_\mu\gamma_5 d)$ and $(\bar{u}\gamma_5 d)$, which has the spectral representation

$$\begin{aligned}\sum_{\vec{z}} e^{i\vec{P}\cdot\vec{z}} \langle [\bar{u}\gamma_\mu\gamma_5 d](\vec{z},t)[\bar{d}\gamma_5 u](0)\rangle \\ = \frac{e^{-E_\pi(\vec{P})t}}{2E_\pi(\vec{P})} Z_\pi(\vec{P}) i f_\pi P_\mu + \ldots,\end{aligned} \tag{1}$$

where f_π is the bare pion decay constant, defined from the ground-state pion-to-vacuum matrix element of the axial-vector current $\langle\Omega|\bar{u}\gamma_\mu\gamma_5 d|\pi(\vec{P})\rangle = i f_\pi P_\mu$, and $Z_\pi(\vec{P}) \equiv \langle\pi(\vec{P})|\bar{d}\gamma_5 u|\Omega\rangle$ is the ground-state overlap factor of the pseudoscalar pion operator. Once there is a large boost in the z-direction, the overlap of $(\bar{u}\gamma_z\gamma_5 d)$ with moving pion states will be enhanced by P_z as in Eq. (1) and dominate the signal.

The overlap between axial-vector and pseudoscalar operators follows from the symmetries of QCD in boosted frames. In the continuum and infinite-volume limits, both pseudoscalar and axial-vector meson operators parallel to the momentum vector, $(\bar{u}\gamma_z\gamma_5 d)$ for $\vec{P} = P_z\hat{e}_z$, transform trivially under the little group of rotations leaving $\vec{P}$ invariant. The exact symmetries of the finite-volume lattice theory form a discrete subgroup of this little group and therefore $(\bar{u}\gamma_5 d)$ and $(\bar{u}\gamma_z\gamma_5 d)$ transform in the same irreps of the lattice symmetry groups for boosted frames. Explicitly, for $\vec{P} = P_z\hat{e}_z$ the cubic group is broken as $O_h \to C_{4v}$, the pseudoscalar irrep subduces as $A_1^- \to A_2$, and the axial-vector irrep subduces as $T_1^+ \to A_2 \oplus E$. It is precisely the $(\bar{u}\gamma_z\gamma_5 d)$ component of $(\bar{u}\gamma_i\gamma_5 d)$ that transforms in the A_2 irrep, confirming that $(\bar{u}\gamma_z\gamma_5 d)$ and $(\bar{u}\gamma_5 d)$ transform identically.

Higher-spin interpolators overlap with lower-spin states in boosted frames only through extra P_μ-dependent kinematic factors as in Eq. (1). At large momentum the overlap of $(\bar{u}\gamma_t\gamma_5 d)$ with the pion ground state is related to that of the $(\bar{u}\gamma_5 d)$ operator by $f_\pi E_\pi / Z_\pi$, which provides an enhancement of $\mathcal{O}(E_\pi^2/m_\pi^2)$ to $(\bar{u}\gamma_t\gamma_5 d)$ two-point correlators relative to $(\bar{u}\gamma_5 d)$ correlators. A similar argument also applies to $(\bar{u}\gamma_z\gamma_5 d)$, where the kinematic enhancement is $\mathcal{O}(P_z^2/m_\pi^2)$, except that this operator has zero overlap with the pion ground state in the rest frame. In general, $(\bar{u}\gamma_\mu\gamma_5 d)$ two-point correlators receive a kinematic enhancement of $\mathcal{O}(P_\mu^2/m_\pi^2)$ at large momentum.

An overall enhancement of the correlator signal does not guarantee an improvement in the SNR, which also requires an analysis of variance correlators following the methods of Parisi and Lepage [24, 25]. For a generic pion interpolator $O_\pi(\vec{x},t)$, the variance correlator associated with $C_\pi(\vec{P},t) \equiv \sum_{\vec{x}} O_\pi(\vec{x},t) O_\pi^\dagger(0) e^{i\vec{P}\cdot\vec{x}}$,

$$\begin{aligned}\mathrm{Var}(C_\pi) &= \left\langle \mathrm{Re}(C_\pi)^2 \right\rangle - \langle C_\pi \rangle^2 \\ &= \frac{1}{2}\left\langle |C_\pi|^2 \right\rangle + \frac{1}{2}\left\langle C_\pi^2 \right\rangle - \langle C_\pi \rangle^2 ,\end{aligned} \tag{2}$$

involves $C_\pi(\vec{P},t)^2$, which includes two-pion states with total momentum $2\vec{P}$, as well as

$$|C_\pi|^2 = \sum_{\vec{x},\vec{y}} e^{i\vec{P}\cdot(\vec{x}-\vec{y})} O_\pi(\vec{y},t) O_\pi^\dagger(\vec{x},t) O_\pi^\dagger(0) O_\pi(0), \tag{3}$$

which has total momentum zero and is dominated at late time by states with two $|\vec{P}| = 0$ pions decaying at a rate $\sim 2m_\pi$, leading to exponential SNR decay for boosted pion states.

For these $|\vec{P}| = 0$ two-pion states, the P_μ^2/m_π^2 factors arising for kinematically-enhanced interpolators are simply equal to unity when they are non-zero. At large t the variance of C_π is not kinematically enhanced, so $\mathrm{SNR}(C_\pi) \equiv \langle C_\pi \rangle / \sqrt{\mathrm{Var}(C_\pi)}$ receives the same $\mathcal{O}(P_\mu^2/m_\pi^2)$ enhancement as the signal $\langle C_\pi \rangle$. Current state-of-the-art continuum-extrapolated parton structure calculations with near-physical pion masses have employed boosts of up to $P_z \sim 1.9$ GeV for parton distribution functions (PDFs) [34] and up to $P_z \sim 2.2$ GeV for a determination of the Collins-Soper kernel [35], corresponding to SNR enhancement factors for two-point correlators as large as $E_\pi^2/m_\pi^2 \sim 200$.

Additional excited-state effects arise from higher-spin states that overlap with $(\bar{u}\gamma_\mu\gamma_5 d)$, which might complicate the extraction of ground-state observables and partially counteract the SNR benefits of kinematically-enhanced interpolators. However, in general, one would expect overlap factors of the kinematically-enhanced interpolators onto single-particle states of mass M_n to be $\propto M_n^{-2}$ and therefore suppressed relative to the ground-state pion by an additional factor $\mathcal{O}(m_\pi^2/M_n^2)$. Thus the contamination could become less significant for the heavier excited states at large boosts.

Previous calculations have used $(\bar{u}\gamma_t\gamma_5 d)$ to calculate the pion distribution amplitude (DA) in a generalized

eigenvalue problem (GEVP) setup [36, 37], but its SNR benefits were not revealed. One reason is that the enhancement factor for pion DA is linear in E_π/m_π, which was not large enough ($\lesssim 5$) in those calculations to provide a noteworthy enhancement. As we show below, $(\bar{u}\gamma_t\gamma_5 d)$ has worse SNR than $(\bar{u}\gamma_5 d)$ for a static pion, which offsets its enhancement at small boosts.

There are similarities between kinematically-enhanced interpolators and operators containing covariant derivatives D_μ, which also lead to overlaps proportional to P_μ [38, 39]. However, D_μ insertions do not lead to enhanced SNR because of two key differences. First, γ_μ is dimensionless and introduces overlap factors of P_μ/m_π while D_μ is dimension 1 and introduces overlap factors of aP_μ; the latter vanishes in the continuum limit while the former approaches a constant that can be much larger than one for large boosts. Second, there is another factor of $\langle x^n\rangle$ introduced by D_μ^n corresponding to the moments of the lightcone distribution amplitude of the hadron, which is usually an order of magnitude smaller than 1 and can be more suppressed for larger n. Together, these effects strongly suggest that operators with D_μ insertions should not be expected to share the kinematic SNR enhancement of $(\bar{u}\gamma_\mu\gamma_5 d)$ operators.

An identical strategy can be used to construct nucleon interpolators using the quark-field "plus" components. The standard interpolator for a static nucleon is

$$N_\Gamma = \epsilon_{abc}(d_a^T C\Gamma u_b)\mathcal{P}_+ u_c, \tag{4}$$

with $\Gamma = \gamma_5$ and C the charge conjugate operator, $\mathcal{P}_\pm \equiv (1 \pm \gamma_t)/2$ to project the positive-parity sector in the rest frame, and ϵ_{abc} the Levi-Civita symbol with a, b, c as color indices. Here, the diquark $(d_a^T C\gamma_5 u_b)$ has spin 0. Conversely, the leading Fock state built from quark-field "plus" components has a spin-1 diquark [23]. The most straightforward case is $\Gamma = \gamma_5\gamma_\mu$,

$$N_{\gamma_5\gamma_\mu} = \epsilon_{abc}(d_a^T C\gamma_5\gamma_\mu u_b)\mathcal{P}_+ u_c, \tag{5}$$

whose overlap with nucleon states takes the form [22, 40]

$$\langle 0|N_{\gamma_5\gamma_\mu}|N(\vec{P})\rangle = \alpha P_\mu \mathcal{P}_+ u(\vec{P}) + \beta\gamma_\mu\mathcal{P}_+ u(\vec{P}), \tag{6}$$

where $u(\vec{P})$ is a free Dirac spinor and α, β are scalar functions of $\vec{P}$. The term proportional to P_μ is not present in $\langle 0|N_{\gamma_5}|N(\vec{P})\rangle = Z(\vec{P})\mathcal{P}_+ u(\vec{P})$ with scalar $Z(\vec{P})$. This term provides $\mathcal{O}(P_\mu^2/M_N^2)$ enhancement for $N_{\gamma_5\gamma_\mu}$ two-point correlators in comparison with N_{γ_5} correlators.

In the rest frame, N_Γ can also be projected by $\mathcal{P}_-$ to isolate the negative-parity sector containing the $N^*(1535)$ resonance. Under boost, parity is no longer a good quantum number, and states boosted from both parity sectors mix with each other. Alternatives to the parity projector $\mathcal{P}_+$ in Eq. (4) are considered in Appendix B, where we also found that the γ_t term in $\mathcal{P}_\pm$ projects the quark with free spinor indices to its u_+ components and thus automatically introduces an $\mathcal{O}(E_N/M_N)$ kinematic enhancement in N_Γ two-point correlators. In the remaining part of this work, we will show results only with $\mathcal{P}_+$ projection.

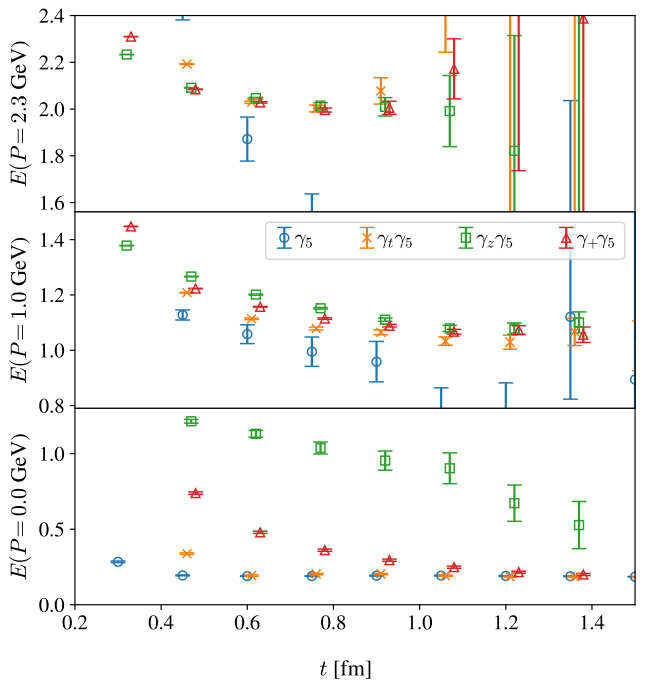

FIG. 1: Comparison of the effective mass of the pion at various boosts with four interpolators. At large momentum, all three kinematically-enhanced interpolators $(\bar{u}\Gamma d)$ with $\Gamma = \{\gamma_t\gamma_5, \gamma_z\gamma_5, \gamma_+\gamma_5\}$ show substantial precision improvements compared with the traditional $(\bar{u}\gamma_5 d)$ interpolators.

Nucleon interpolators with $\Gamma = \gamma_\mu$ overlap with negative-parity states in the rest frame but also transform identically to N_Γ in boosted frames where γ_μ is parallel to P_μ. Their overlaps take the form [40, 41]

$$\langle 0|N_{\gamma_\mu}|N(\vec{P})\rangle = \alpha' P_\mu\gamma_5\mathcal{P}_+ u(\vec{P}) + \beta'\gamma_\mu\gamma_5\mathcal{P}_+ u(\vec{P}), \tag{7}$$

and therefore include kinematic enhancement analogous to $N_{\gamma_5\gamma_\mu}$. Both $N_{\gamma_5\gamma_\mu}$ and N_{γ_μ} overlap with spin-$\frac{3}{2}$ baryons, such as the $\Delta(1232)$ [42], but the overlap is found below to be numerically small at large momentum.

Parisi-Lepage analysis analogous to the pion case above shows that the boosted nucleon variance is dominated by states with three zero-momentum pions with energies $\sim 3m_\pi$ that do not receive kinematic enhancements, and therefore the $N_{\gamma_5\gamma_\mu}$ and N_{γ_μ} correlator SNR should receive $\mathcal{O}(P_\mu^2/M_N^2)$ enhancement.

Lattice QCD verification — We test these new interpolators numerically on a gauge ensemble produced by the MILC collaboration [43] with 2+1+1 flavors of highly improved staggered quarks (HISQ) tuned to reproduce the physical pion mass and the one-loop Symanzik improved gauge action [44]. The lattice has a volume $L^3 \times T = 32^3 \times 48$ and lattice spacing $a \approx 0.15$ fm. We apply two steps of HYP smearing with parameters

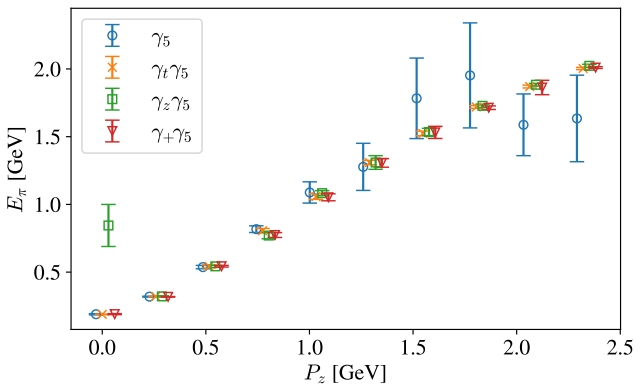

FIG. 2: The ground-state energy of the pion extracted using the Lanczos method at various boosts for the interpolators $(\bar{u}\Gamma d)$ with $\Gamma = \{\gamma_5, \gamma_t\gamma_5, \gamma_z\gamma_5, \gamma_+\gamma_5\}$. As in Fig. 1, the precision is substantially improved at large momentum when using the kinematically-enhanced interpolators $(\bar{u}\gamma_\mu\gamma_5 d)$. Note that for systems at rest, $(\bar{u}\gamma_z\gamma_5 d)$ has zero overlap with the pion.

$\{\alpha_1, \alpha_2, \alpha_3\} = \{0.75, 0.6, 0.3\}$ [45] to the gauge fields and then use a Wilson-clover action [46] for the valence quarks with $c_{\rm SW} = 1$ and $\kappa = 0.12635$, tuned to produce ≈ 190 MeV pions. We perform measurements with 64 source locations on 334 configurations. To increase the signal at large momentum, we use momentum smearing of $k \approx 1.55$ GeV for pion momentum from $P_z = 0$ to $P_z = 2.32$ GeV [21].

Figure 1 confirms significant SNR improvement in the effective masses $E_{\rm eff}(t,P) \equiv 1/a \ln[C(t,P)/C(t+a,P)]$ of $(\bar{u}\gamma_\mu\gamma_5 d)$ interpolators at large momenta. It is clear that $(\bar{u}\gamma_z\gamma_5 d)$ only overlaps with heavier states at $P_z = 0$ but becomes dominated by pion states at large momenta. At the largest momentum, $P_z \sim 2.32$ GeV, $(\bar{u}\gamma_5 d)$ correlators become very noisy for $t \gtrsim 0.6$ fm and decrease to unphysical values, which is a clear sign of noise dominance; however, $(\bar{u}\gamma_\mu\gamma_5 d)$ interpolators can achieve reliable signals out to larger $t \sim 0.9$ fm.

Besides $(\bar{u}\gamma_z\gamma_5 d)$ and $(\bar{u}\gamma_t\gamma_5 d)$, we compute correlators for $(\bar{u}\gamma_+\gamma_5 d)$ operators that can be directly associated with the leading lightcone Fock states of the pion as discussed above and in Ref. [23]. When the two interpolators $(\bar{u}\gamma_t\gamma_5 d)$ and $(\bar{u}\gamma_z\gamma_5 d)$ have equal quality, there is an extra factor-of-2 enhancement in the signal for $(\bar{u}\gamma_+\gamma_5 d)$, while the noise does not increase as much due to their correlations, resulting in a slightly better SNR than either component. In general, we observe the SNRs follow the ordering $\mathrm{SNR}(\bar{u}\gamma_+\gamma_5 d) > \mathrm{SNR}(\bar{u}\gamma_z\gamma_5 d) > \mathrm{SNR}(\bar{u}\gamma_t\gamma_5 d)$ at large momenta.

Excited-state effects in Fig. 1 are consistent with the theoretical expectations above. At small momentum, $(\bar{u}\gamma_\mu\gamma_5 d)$ correlators converge slower than $(\bar{u}\gamma_5 d)$, indicating larger excited-state effects. At large momentum where additional excited-state effects are kinematically suppressed, $(\bar{u}\gamma_\mu\gamma_5 d)$ converges faster. In a naïve implementation, the operators $(\bar{u}\gamma_z\gamma_5 d)$ and $(\bar{u}\gamma_+\gamma_5 d)$ work best for large momentum, but $(\bar{u}\gamma_t\gamma_5 d)$ is more suitable to scan a large range of momenta. A strategy for removing excited-state contamination from $(\bar{u}\gamma_z\gamma_5 d)$ correlation functions by forming differences with correlation functions built from a transverse component, e.g., $(\bar{u}\gamma_x\gamma_5 d)$, is presented in Appendix C.

We extract the ground-state energy $E_\pi(P_z)$ from the two-point correlators with the Lanczos method [26–28] using nested bootstrap median estimators and spurious-state filtering with the ZCW test with $F_{\rm ZCW} = 10$ [28]. Terms arising from Wick's theorem specifically at $t = 0$, see Appendix D, have significant effects on $(\bar{u}\gamma_z\gamma_5 d)$ and $(\bar{u}\gamma_+\gamma_5 d)$ correlators and without including them the spectral representations are badly violated and the Lanczos algorithm breaks down. A straightforward workaround is to include one application of the transfer matrix in the Lanczos initial state, i.e., start the analysis at $t = 2$. Lanczos then converges within a few iterations; results after 22 iterations, incorporating $t \in [2, T-3]$, are shown in Fig. 2. For $P_z = 0$, the ground state identified from $(\bar{u}\gamma_z\gamma_5 d)$ correlators is significantly heavier than the pion mass, as expected due to its T_1^+ quantum numbers. For non-zero momenta, all correlators provide statistically consistent ground-state energy estimates. As the momentum increases, the kinematically-enhanced interpolators clearly show growing SNR improvement compared to the traditional $(\bar{u}\gamma_5 d)$ interpolator. The improvement is consistent with $\mathcal{O}(P_\mu^2/m_\pi^2)$ scaling for all but the smallest momenta and reaches factors of $\sim$ 30-50 for $P_z > 2$ GeV. Appendix A provides another way to estimate the enhancement as a function of P_z/m_π, where we have also included data with a heavier pion mass $m_\pi \approx 400$ MeV to show the scaling. It demonstrates an improvement factor of up to ~ 50 that is consistent with the Lanczos analysis.

We measure the nucleon two-point correlators on the same lattice with 16 sources and 202 configurations. To reach higher momentum, we take lattice momenta along the diagonal, $P = \frac{2\pi n}{L} \times (1,1,1)$ for $n \in [0,7]$, i.e. up to 3.1 GeV. The momentum smearing is optimized for the largest momentum $P = 3.1$ GeV. Figure 3 shows the effective mass plot for static and boosted correlators with the five different operators N_Γ where $\Gamma \in \{\gamma_5, \gamma_5\gamma_t, \gamma_5\gamma_z, \gamma_t, \gamma_z\}$.[1] All four kinematically-enhanced interpolators show similar SNR improvement compared to N_{γ_5} at large momentum. Among them, $N_{\gamma_5\gamma_t}$ has the least excited-state contamination where differences are visible.

Unlike the pion case where the pseudoscalar interpola-

[1] For the general case of a boost with momentum $\vec{P}$ not necessarily aligned with the z-axis, the spatial gamma matrix would take the form of $\vec{\gamma}\cdot\hat{P}$. In the specific case of the momentum $\vec{P} \propto (1,1,1)$ used here, the projector is $\Gamma = (\gamma_x + \gamma_y + \gamma_z)/\sqrt{3}$. However, for simplicity, we give the projectors for the case of momentum in the z-direction rather than the somewhat more involved forms actually used for off-axis momenta.

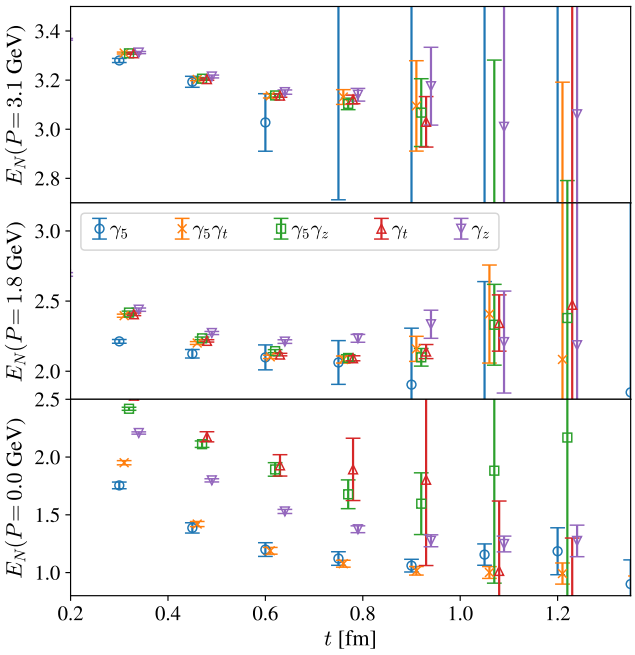

FIG. 3: The analog of Fig. 1 for the nucleon, where the interpolating operators are $(d^T C\Gamma u)\mathcal{P}_+ u$ with $\Gamma = \{\gamma_5, \gamma_5\gamma_t, \gamma_5\gamma_z, \gamma_t, \gamma_z\}$. At large momentum, the last four operators all yield higher precision than the choice of $\Gamma = \gamma_5$.

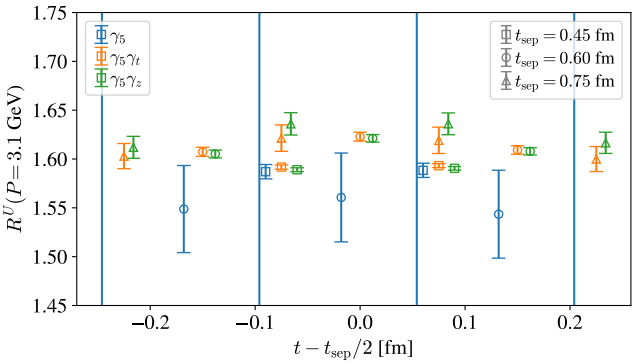

FIG. 4: A ratio of three-point to two-point correlation functions using three of the nucleon interpolators in Fig. 3. The precision is improved when using the kinematically-enhanced interpolators with $\Gamma = \{\gamma_5\gamma_t, \gamma_5\gamma_z\}$ as opposed to the choice of $\Gamma = \gamma_5$.

tor is optimal in the rest frame, the SNR for the nucleon interpolator $N_{\gamma_5\gamma_t}$ is equally good as N_{γ_5} at $P = 0$. At large momentum, the enhancement factor is of similar size to E_N^2/M_N^2 without the $\mathcal{O}(1)$ loss that appears in the pion case. Lanczos analysis of the nucleon correlators with the same spurious-state filtering as above gives a ground-state energy estimator with SNR enhanced by factors of 3–10 for the kinematically-enhanced interpolators in comparison with N_{γ_5}. With larger ϵ_{ZCW}, Lanczos analysis of N_{γ_5} leads to more precise signals but of a higher-energy state than that resolved from the kinematically-enhanced interpolators.

The kinematic enhancement applies exactly the same way in the three-point correlators. For an illustration, we measure the bare unpolarized quark quasi-PDF matrix element [9] $h_B^U(z, P_z)$ of the nucleon at $z = 0$ for up quark connected diagrams, corresponding to the matrix element of the vector current in the nucleon state,

$$C_{3\mathrm{pt}}(\vec{P}, t, t_{\mathrm{sep}}) = \sum_{\vec{x}} e^{i\vec{x}\cdot\vec{P}} \mathrm{Tr}\left[\mathcal{P}_+ \langle N_\Gamma(t_{\mathrm{sep}}, \vec{x}) \times \overline{u}(t)\gamma_t u(t)\ \overline{N}_\Gamma(0)\rangle\right], \quad (8)$$

which has the same kinematic enhancement as the two-point correlators. Thus we take the ratio

$$R^U(t, t_{\mathrm{sep}}) = \frac{C_{3\mathrm{pt}}(t, t_{\mathrm{sep}})}{C_{2\mathrm{pt}}(t_{\mathrm{sep}})} = h_B^U(0, P_z) + \ldots, \quad (9)$$

where the omitted terms are contamination from excited states. We show the results at $P = 3.1$ GeV in Fig. 4. The results are consistent among the three operators, and we clearly observe a significant improvement with the new interpolators at the level of correlators, especially for larger t_{sep} where the ground states are dominating. The ratios for the same t_{sep} are almost flat in t and converge nicely for $t_{\mathrm{sep}} \geq 0.6$ fm, implying suppressed excited state contamination. This is consistent with the effective mass in Fig. 3 where the plateau is reached for $t > 0.6$ fm.

Conclusion — In this work, we propose interpolating operators for lattice QCD calculations of highly-boosted pions and nucleons with kinematically-enhanced ground-state overlap factors at large momentum. The signal of lattice correlators is enhanced quadratically in the Lorentz boost factor, while the noise is insensitive to the momentum, resulting in a kinematically-enhanced SNR. Compared to the traditional interpolators, we find an improvement in the SNR by up to ~ 50 for pions with $P_\mu^2/m_\pi^2 \approx 150$, and up to ~ 10 for nucleons with $P_\mu^2/M_N^2 \approx 10$, which correspond to increases of statistics by $\mathcal{O}(2000)$ and $\mathcal{O}(100)$, respectively. Using these new interpolators will tremendously reduce the cost of measuring boosted hadron spectra and matrix elements, significantly improving the precision of lattice calculations of form factors at large Q^2 and partonic observables. Such high-precision, high-momentum lattice calculations of form factors and parton distributions are necessary inputs for analyzing collider experiments, including the LHC and the upcoming Electron-Ion Collider. Moreover, they could potentially be extended to processes such as $\pi\pi$ scattering and B meson decays to energetic pions, which are essential to resolve CP matrix elements for high-precision unitary violation searches.

Acknowledgments

We thank Artur Avkhadiev, Yang Fu, Jinchen He, Xiangdong Ji, Luchang Jin, Andreas Kronfeld, Yushan Su, and Ruth Van de Water for valuable discussions. This material is based upon work supported by the U.S. Department of Energy, Office of Science, Office of Nuclear Physics through Contract No. DE-AC02-06CH11357, the Scientific Discovery through Advanced Computing (SciDAC) award *Fundamental Nuclear Physics at the Exascale and Beyond*, the Quark-Gluon Tomography (QGT) Topical Collaboration under contract no. DE-SC0023646, and the Fermi Research Alliance, LLC under Contract No. DE-AC02-07CH11359 with the U.S. Department of Energy, Office of Science, Office of High Energy Physics. Argonne National Laboratory's contribution is also based upon work supported by Laboratory Directed Research and Development (LDRD) funding from Argonne National Laboratory, provided by the Director, Office of Science, of the U.S. Department of Energy under Contract No. DE-AC02-06CH11357. We gratefully acknowledge the computing resources provided on Swing, a high-performance computing cluster operated by the Laboratory Computing Resource Center at Argonne National Laboratory. This research used resources of the Argonne Leadership Computing Facility, a U.S. Department of Energy (DOE) Office of Science user facility at Argonne National Laboratory and is based on research supported by the U.S. DOE Office of Science-Advanced Scientific Computing Research Program, under Contract No. DE-AC02-06CH11357. This research also used facilities of the USQCD Collaboration, which are funded by the Office of Science of the U.S. Department of Energy. Our calculation is performed using the GLU [47] and QUDA [48] software packages.

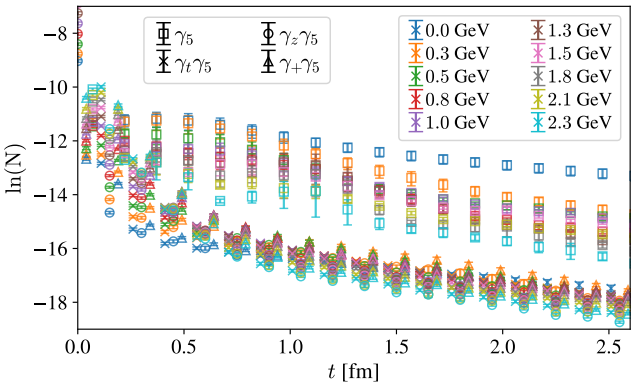

FIG. 5: The scaling of the noise N, defined as the standard deviation of the correlation function, as a function of source-sink separation at various momenta. In all cases, $\mathrm{N} \propto e^{-m_\pi t}$ asymptotically, but the prefactor is much smaller for the improved interpolators $(\bar{u}\gamma_\mu\gamma_5 d)$.

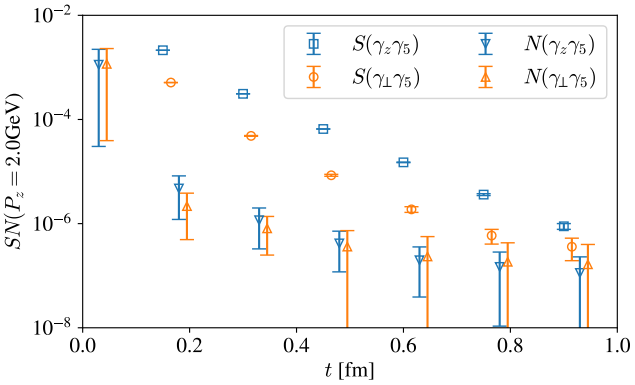

FIG. 6: A comparison of the signal S and noise N, defined as the mean value and standard deviation of the correlation function, for the meson boosted in the z-direction using interpolators $(\bar{u}\gamma_z\gamma_5 d)$ and $(\bar{u}\gamma_x\gamma_5 d)$. Both have comparable noise, but the z-aligned interpolator leads to a substantial enhancement in the signal.

Appendix A: Quantitative analysis of the kinematic enhancement

To quantify the improvement of the new pion interpolators, in principle we need to take a ratio of the SNR among them. However, since the signal of the traditional interpolator $(\bar{u}\gamma_5 d)$ quickly decays to the noise-dominant region, its SNR becomes just a constant $\mathcal{O}(1)$ fluctuation. Thus it is not a faithful comparison beyond 0.45 fm for large momentum. At this early Euclidean time, the correlators may not yet be dominated by the ground state pion, so a direct SNR comparison will not accurately reflect the enhancement in pion. However, we notice that the noise $\mathrm{N}(\bar{u}\Gamma d)$ follows a nice asymptotic cosh-like behavior with the ground-state pion mass, as shown in Fig. 5. The kinematic enhancement only exists in the signal but not in the noise, as shown by a comparison between $(\bar{u}\gamma_z\gamma_5 d)$ and $(\bar{u}\gamma_x\gamma_5 d)$ in Fig. 6. In both plots, we estimate the uncertainty of the noise from the variance of the noise calculated in each jackknife sample with $n-1$ configurations. Since the fluctuations in the noise are more stable at large t, a quantitative comparison is more reliable for the noise measurements themselves. If we can match the corresponding signals to the same level, then the comparison of noise will be equivalent to the comparison of the actual SNR.

To realize this goal, we utilize the fact that the ground state signal falls off in the same asymptotic form among different interpolating operators, except for $(\bar{u}\gamma_z\gamma_5 d)$ at rest. Thus, on a logarithmic scale, they just differ by a vertical shift at large t. More specifically, the shift can be estimated through the partially conserved axial current (PCAC) relation [49],

$$\langle\pi|\bar{d}\gamma_5 u|\Omega\rangle \approx \frac{1}{m_l}\partial^\mu\langle\pi|\bar{d}\gamma_\mu\gamma_5 u|\Omega\rangle \approx \frac{i f_\pi m_\pi^2}{m_l}, \qquad \text{(A1)}$$

where m_l is the light quark mass, indicating that asymp-

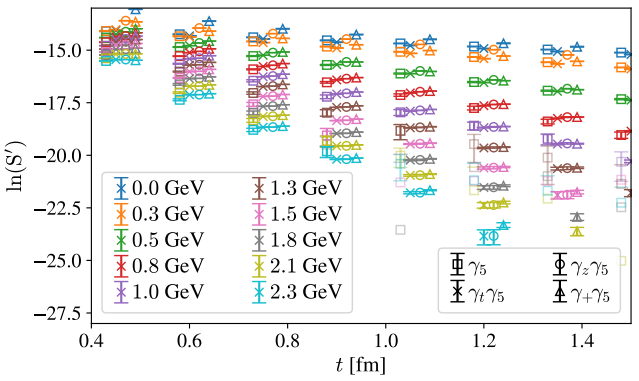

FIG. 7: The rescaled signal S′ for four pion correlators with different interpolators, defined as the signal S multiplied by a time-independent factor such that S′ is comparable for all interpolators at early time. At fixed momentum, all correlators decay at the same rate, so S′ remains independent of the choice of interpolator even at late time, until the point where the signal is lost to noise.

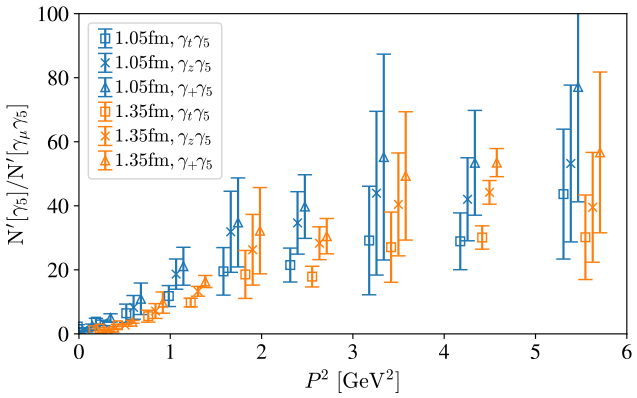

FIG. 8: The ratio of rescaled noises, $\mathrm{N}'(\bar{u}\gamma_5 d)/\mathrm{N}'(\bar{u}\gamma_\mu\gamma_5 d)$, for 190 MeV pion interpolators. We can achieve noise reduction by a factor of ~ 50 at $P_z \approx 2.32$ GeV, which corresponds to an $\mathcal{O}(2000)$-fold increase in statistics. The $(\bar{u}\gamma_+\gamma_5 d)$ performs best among the axial vector interpolators at large momenta.

totically,

$$\mathrm{S}(\bar{u}\gamma_5 d) \approx \frac{m_\pi^2}{m_l^2}\frac{m_\pi^2}{P_\mu^2}\mathrm{S}(\bar{u}\gamma_\mu\gamma_5 d). \tag{A2}$$

Although the relation is not exact and the quark mass is unknown, we can use a one-parameter model to approximate the data,

$$\mathrm{S}(\bar{u}\gamma_5 d) \approx \mathrm{S}'(\bar{u}\gamma_\mu\gamma_5 d) \equiv \mathrm{S}(\bar{u}\gamma_\mu\gamma_5 d) \times \lambda \times \frac{m_\pi^2}{P_\mu^2}, \tag{A3}$$

where the free parameter $\lambda \approx \frac{m_\pi^2}{m_l^2}$ can still be momentum- and smearing-dependent. But we find that with a fixed $\lambda = e^{4.2} \approx 67$, the scaled correlators $\mathrm{S}'(\bar{u}\gamma_\mu\gamma_5 d)$ are consistent with $\mathrm{S}(\bar{u}\gamma_5 d)$ before noise dominance at all momenta, as shown in Fig. 7. Then we can quantitatively compare the SNR by taking a ratio of their noises including the factor $\lambda m_\pi^2/P_\mu^2$,

$$\frac{\mathrm{SNR}(\bar{u}\gamma_\mu\gamma_5 d)}{\mathrm{SNR}(\bar{u}\gamma_5 d)} \approx \frac{\mathrm{N}'(\bar{u}\gamma_5 d)}{\mathrm{N}'(\bar{u}\gamma_\mu\gamma_5 d)} \equiv \frac{P_\mu^2}{\lambda m_\pi^2}\frac{\mathrm{N}(\bar{u}\gamma_5 d)}{\mathrm{N}(\bar{u}\gamma_\mu\gamma_5 d)}. \tag{A4}$$

Figure 8 shows the ratio of rescaled noises for two large time slices, which is a good approximation to $\mathrm{SNR}(\bar{u}\gamma_\mu\gamma_5 d)/\mathrm{SNR}(\bar{u}\gamma_5 d)$. The improvement clearly grows in an almost-linear pattern with P^2. At the largest momentum $P_z = 2.3$ GeV, the improvement in signal-to-noise ratio can be a factor as large as 40 to 50, consistent with the Lanczos results, corresponding to an increase of statistics by a factor of $\mathcal{O}(2000)$. The final enhancement factor is roughly 1/3 of the kinematic factor P_z^2/m_π^2 due to the loss of overlap with pion for the $(\bar{u}\gamma_t\gamma_5 d)$ operator compared to the $(\bar{u}\gamma_5 d)$ in the rest frame. Note that this is still for a heavier pion of mass around 190 MeV, which is already 1.4 times the physical value. Taking this

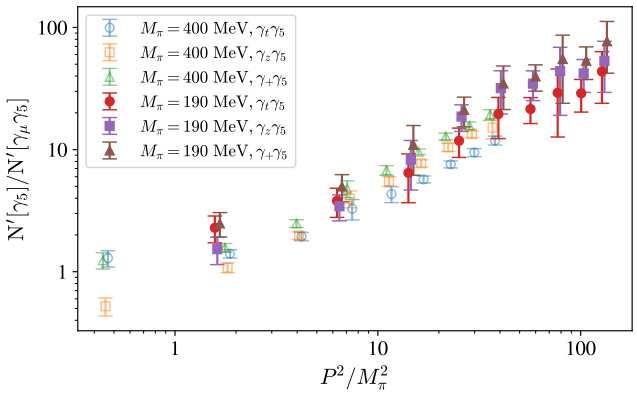

FIG. 9: The ratio of noise between the rescaled noise, $\mathrm{N}'(\bar{u}\gamma_5 d)/\mathrm{N}'(\bar{u}\gamma_\mu\gamma_5 d)$, compared to the predicted enhancement factor P^2/M_π^2. This relation is linear on a log-log plot, indicating that the predicted enhancement is correct up to a constant $\mathcal{O}(1)$ factor. Notably, the data at two different pion masses (190 MeV and 400 MeV) lie on the same line, giving support to the theoretical prediction that the enhancement factor scales inversely with m_π^2.

factor into account, the potential improvement on phyiscal pion measurements can potentially reach a factor of $\mathcal{O}(10^4)$ increase in statistics at the same momentum.

To confirm that the kinematic enhancement works better for lighter pion masses, we perform the same measurement with valence pion mass $m_\pi \approx 400$ MeV, roughly twice that of the previous test. Following the same procedure, we find the scaling in P_z^2/m_π^2 to be the same as the lighter pion case, and the enhancement factor to be about 4 times smaller at the same P_z, as shown in Fig. 9.

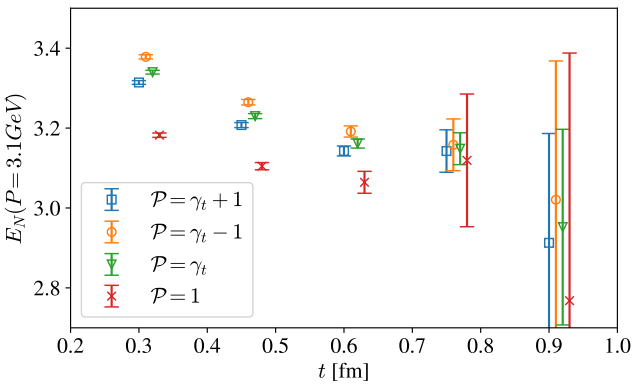

FIG. 10: The effective mass plot of the nucleon two-point correlators at a boost of 3.1 GeV using various parity projectors.

Appendix B: Baryon interpolator spin projections

According to the analysis above, the ψ_+ component of the spinor ψ is kinematically enhanced in a boosted frame. The same enhancement also applies to the free quark spinor in the nucleon interpolator. In a nucleon two-point contraction, the projection operator always appears in the following structure:

$$\langle N|N\rangle = c_1 \mathrm{Tr}[\mathcal{P}S_1] + c_2 \mathrm{Tr}[S_3 \mathcal{P} S_2 \dots], \tag{B1}$$

where S_i are quark propagators with $i \in \{1,2,3\}$ labeling the three quark fields in the nucleon interpolator, and the $\dots$ represents some more complicated spin structure determined by the diquark. As long as the projection operator $\mathcal{P}$ is multiplied to the quark propagators on both sides, the quark propagator can be re-written as the Wick contraction of the spinor fields $S \sim \psi\bar{\psi}$. This indicates that there is always a sub-structure $\bar{\psi}_1 \mathcal{P} \psi_2$ in the trace

$$\langle N|N\rangle = \mathrm{Tr}[\bar{\psi}_1 \mathcal{P} \psi_2 \dots], \tag{B2}$$

which is just like a meson. Thus the γ_t component in $\mathcal{P}$ will project out the $\psi_\pm$ component of the two adjacent quark fields $\bar{\psi}\gamma_t\psi = \bar{\psi}_+\gamma_+\psi_+/\sqrt{2}$, introducing a kinematic enhancement factor of E/M to the correlator. As a result, the contribution from γ_t at large momentum becomes more precise than the contribution from the other component (the identity). Figure 10 shows the comparison among different projecting operators.

One can tell that the projection operators with a γ_t component are cleaner than $\mathcal{P}=1$. Since $\gamma_t = \mathcal{P}_+ - \mathcal{P}_-$ comes from a linear combination of two different parity projections in the rest frame, it contains more contamination from negative parity states than $\mathcal{P}_+$ but less than $\mathcal{P}_-$.

Note that the $\mathcal{P}_+$ projection is positive definite by definition of the lattice correlator, while $\mathcal{P}_-$ is negative definite. So only $\mathcal{P}_+$, $-\mathcal{P}_-$, and $\gamma_t = \mathcal{P}_+ - \mathcal{P}_-$ project out positive-definite correlators, where all excited states contribute with the same sign. On the other hand, $1 = \mathcal{P}_+ + \mathcal{P}_-$ projection contains excited state contribution with indefinite signs thus may result in a fake plateau in the effective mass, the same as in correlators with asymmetric source-sink interpolators. One needs to be more careful when analyzing correlators with this projection.

Appendix C: Excited-state suppression for the pion

In the continuum, infinite-volume limit, there are two sets of excited-state contamination in the higher-spin interpolators. For example, the two-point correlator of two axial-vector interpolators contains two different spin components,

$$\langle[\bar{u}\gamma_\mu\gamma_5 d]^\dagger[\bar{u}\gamma_\nu\gamma_5 d]\rangle = \sum_{n,S=1}\left(\frac{P_\mu P_\nu}{M_{n,1}^2} - g_{\mu\nu}\right)C_{n,1} + \sum_{n,S=0}\frac{P_\mu P_\nu}{M_{n,0}^2}C_{n,0}, \tag{C1}$$

where M_n is the invariant mass of the nth state. Taking both indices to be $\{t, z, \perp\}$, we find that

$$\begin{aligned}
\langle[\bar{u}\gamma_t\gamma_5 d]^\dagger[\bar{u}\gamma_t\gamma_5 d]\rangle &= \sum_{n,S=1}\frac{P_z^2}{M_{n,1}^2}C_{n,1} + \sum_{n,S=0}\frac{E^2}{M_{n,0}^2}C_{n,0},\\
\langle[\bar{u}\gamma_z\gamma_5 d]^\dagger[\bar{u}\gamma_z\gamma_5 d]\rangle &= \sum_{n,S=1}\frac{E^2}{M_{n,1}^2}C_{n,1} + \sum_{n,S=0}\frac{P_z^2}{M_{n,0}^2}C_{n,0},\\
\langle[\bar{u}\gamma_\perp\gamma_5 d]^\dagger[\bar{u}\gamma_\perp\gamma_5 d]\rangle &= \sum_{n,S=1}C_{n,1}.
\end{aligned} \tag{C2}$$

Compared to the ground-state enhancement, at very large momentum, both $(\bar{u}\gamma_t\gamma_5 d)$ and $(\bar{u}\gamma_z\gamma_5 d)$ correlators have suppressed excited-state contamination of order $\frac{m_\pi^2}{M_n^2}$ regardless of spin. But when the momentum is not significantly higher than excited states—for example, around 1 GeV—the correlator formed from $(\bar{u}\gamma_t\gamma_5 d)$ receives more contamination $\propto \frac{m_\pi^2 E_{n,0}^2}{E_\pi^2 M_{n,0}^2}$ from spin-0 states, and that formed from $(\bar{u}\gamma_z\gamma_5 d)$ receives more contamination $\propto \frac{m_\pi^2 E_{n,1}^2}{P_z^2 M_{n,1}^2}$ from spin-1 states.

If we subtract the transverse counterpart in the correlator, we obtain

$$\langle[\bar{u}\gamma_z\gamma_5 d]^\dagger[\bar{u}\gamma_z\gamma_5 d]\rangle - \langle[\bar{u}\gamma_x\gamma_5 d]^\dagger[\bar{u}\gamma_x\gamma_5 d]\rangle = \sum_{n,S=1}\frac{P_z^2}{M_{n,1}^2}C_{n,1} + \sum_{n,S=0}\frac{P_z^2}{M_{n,0}^2}C_{n,0}, \tag{C3}$$

which remains positive definite (up to lattice artifacts, finite-volume effects, and statistical fluctuations), and also has a more suppressed excited-state contamination $\propto \frac{m_\pi^2}{M_n^2}$ at all momenta regardless of the spin of excited states. This suppression can reach $\mathcal{O}(10^{-2})$ for physical

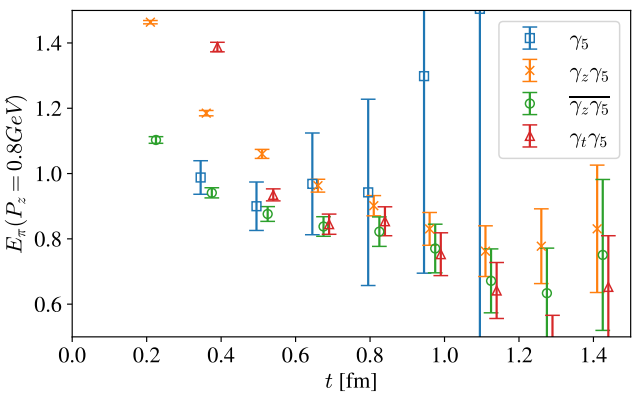

FIG. 11: The effective mass plot of the pion two-point correlators at a boost of 0.8 GeV using various interpolators. At this moderate momentum, there is still obvious excited-state contamination from the axial-vector states in $(\bar{u}\gamma_z\gamma_5 d)$. However, the subtracted correlator, denoted by $\overline{\gamma_z\gamma_5}$, gives a good enhancement in the signal-to-noise ratio and also well-controlled excited-state contamination.

pion, thus allowing an efficient extraction of the ground-state information, at the price of increasing the error by a factor of $\sqrt{2}$ that can be compensated by the large kinematic enhancement.

We test on a data set with both $(\bar{u}\gamma_z\gamma_5 d)$ and $(\bar{u}\gamma_x\gamma_5 d)$ interpolators and find excellent elimination of the axial-vector excited state, as shown in Fig. 11. The $\overline{\gamma_z\gamma_5}$ interpolator, defined as $(\bar{u}\gamma_z\gamma_5 d)$ after subtracting the transverse component, gives rise to correlators that show both significantly improved SNR and more suppressed excited state contamination. It may be useful in the study of heavy meson decays or $\pi\pi$ scattering, where the pion momentum is usually below 1 GeV.

Appendix D: Wick contraction contact terms

Pion correlators for interpolators with generic Dirac structures $(\overline{u}\Gamma d)$ take the form

$$C_\pi(\vec{P},t) = \sum_{\vec{x}} e^{i\vec{P}\cdot\vec{x}} \left\langle \overline{u}(t,\vec{x})\Gamma d(t,\vec{x})\overline{d}(0)\overline{\Gamma}u(0)\right\rangle , \quad \text{(D1)}$$

where $\overline{\Gamma} \equiv \gamma_4\Gamma^\dagger\gamma_4$ and in this section $\langle\cdot\rangle$ denotes an expectation over fermionic degrees of freedom in some fixed gauge-field configuration. Applying Wick's theorem to this time-ordered products of fields gives

$$\begin{aligned} C_\pi(\vec{P},t) = -\sum_{\vec{x}} e^{i\vec{P}\cdot\vec{x}} \mathrm{Tr}\Big[& S_u(\vec{x},t;0)\Gamma S_d(\vec{x},t;0)\overline{\Gamma} \\ & - \left\langle \mathcal{N}[d(\vec{x},t),\overline{d}(0)]\right\rangle \overline{\Gamma} S_u(\vec{x},t;0)\Gamma \\ & + \left\langle \mathcal{N}[\overline{u}(\vec{x},t),u(0)]\right\rangle \Gamma S_d(\vec{x},t;0)\overline{\Gamma}\Big] , \end{aligned} \quad \text{(D2)}$$

where $\mathcal{N}$ denotes any finite-temperature definition of "normal ordering" as described in Ref. [50]. These expectation values of normal-ordered terms vanish for any fields with distinct spacetime arguments [50], giving

$$\begin{aligned} C_\pi(\vec{P},t) = -\sum_{\vec{x}} e^{i\vec{P}\cdot\vec{x}} \mathrm{Tr}\big[& S_u(\vec{x},t;0)\Gamma S_d(\vec{x},t;0)\overline{\Gamma} \\ & + \delta_{0t}\left\langle \mathcal{N}[\overline{u}(0),u(0)]\right\rangle \Gamma S_d(0;0)\overline{\Gamma} \\ & -\delta_{0t}\left\langle \mathcal{N}[d(0),\overline{d}(0)]\right\rangle \overline{\Gamma} S_u(0;0)\Gamma\big] . \end{aligned} \quad \text{(D3)}$$

At zero temperature, the normal-ordered expectation values become vacuum expectation values of fermion anticommutators, which can be explicitly evaluated using Eq. (12) of Ref. [51]. Antisymmetry of these anticommutators causes the two normal-ordered terms to add constructively in Eq. (D3) and provide equal contributions in the isospin limit. At non-zero temperature, they are more complicated to evaluate.

Without explicitly evaluating and including the normal-ordered terms in Eq. (D3), $C_\pi(\vec{P},t)$ can be identified with the usual expression $-\sum_{\vec{x}} e^{i\vec{P}\cdot\vec{x}}\mathrm{Tr}[S_u(\vec{x},t;0)S_d(\vec{x},t;0)]$ if and only if $t > 0$. Note that this result only assumes that the valence quark fields are fermionic operators and holds for arbitrary discretization choices, even mixed/smeared actions, and the fact that $C_\pi(\vec{P},0) \neq -\sum_{\vec{x}} e^{i\vec{P}\cdot\vec{x}}\mathrm{Tr}[S_u(\vec{x},0;0)S_d(\vec{x},0;0)]$ is distinct from other concerns about "contact terms" arising from lattice-scale nonlocality in the action.

[1] J. Koponen, A. C. Zimermmane-Santos, C. T. H. Davies, G. P. Lepage, and A. T. Lytle, Phys. Rev. D **96**, 054501 (2017), 1701.04250.
[2] A. J. Chambers et al. (QCDSF, UKQCD, CSSM), Phys. Rev. D **96**, 114509 (2017), 1702.01513.
[3] C. T. H. Davies, J. Koponen, P. G. Lepage, A. T. Lytle, and A. C. Zimermmane-Santos (HPQCD), PoS **LATTICE2018**, 298 (2018), 1902.03808.
[4] H.-T. Ding, X. Gao, A. D. Hanlon, S. Mukherjee, P. Petreczky, Q. Shi, S. Syritsyn, R. Zhang, and Y. Zhao (2024), 2404.04412.
[5] K.-F. Liu and S.-J. Dong, Phys. Rev. Lett. **72**, 1790 (1994), hep-ph/9306299.
[6] W. Detmold and C. J. D. Lin, Phys. Rev. D **73**, 014501 (2006), hep-lat/0507007.
[7] V. Braun and D. Müller, Eur. Phys. J. C **55**, 349 (2008), 0709.1348.
[8] A. J. Chambers, R. Horsley, Y. Nakamura, H. Perlt, P. E. L. Rakow, G. Schierholz, A. Schiller, K. Somfleth, R. D. Young, and J. M. Zanotti, Phys. Rev. Lett. **118**, 242001 (2017), 1703.01153.
[9] X. Ji, Phys. Rev. Lett. **110**, 262002 (2013), 1305.1539.
[10] X. Ji, Sci. China Phys. Mech. Astron. **57**, 1407 (2014), 1404.6680.

[11] A. V. Radyushkin, Phys. Rev. D **96**, 034025 (2017), 1705.01488.
[12] Y.-Q. Ma and J.-W. Qiu, Phys. Rev. Lett. **120**, 022003 (2018), 1709.03018.
[13] W. Detmold, A. V. Grebe, I. Kanamori, C. J. D. Lin, R. J. Perry, and Y. Zhao (HOPE), Phys. Rev. D **104**, 074511 (2021), 2103.09529.
[14] X. Ji, Y.-S. Liu, Y. Liu, J.-H. Zhang, and Y. Zhao, Rev. Mod. Phys. **93**, 035005 (2021), 2004.03543.
[15] M. Constantinou et al. (2022), 2202.07193.
[16] X. Gao, A. D. Hanlon, S. Mukherjee, P. Petreczky, P. Scior, S. Syritsyn, and Y. Zhao, Phys. Rev. Lett. **128**, 142003 (2022), 2112.02208.
[17] Z. Fan, W. Good, and H.-W. Lin, Phys. Rev. D **108**, 014508 (2023), 2210.09985.
[18] F. Yao et al. (Lattice Parton), Phys. Rev. Lett. **131**, 261901 (2023), 2208.08008.
[19] D. S. Roberts, W. Kamleh, D. B. Leinweber, M. S. Mahbub, and B. J. Menadue, Phys. Rev. D **86**, 074504 (2012), 1206.5891.
[20] M. Della Morte, B. Jaeger, T. Rae, and H. Wittig, Eur. Phys. J. A **48**, 139 (2012), 1208.0189.
[21] G. S. Bali, B. Lang, B. U. Musch, and A. Schäfer, Phys. Rev. D **93**, 094515 (2016), 1602.05525.
[22] M. Burkardt, X.-d. Ji, and F. Yuan, Phys. Lett. B **545**, 345 (2002), hep-ph/0205272.
[23] X.-d. Ji, J.-P. Ma, and F. Yuan, Eur. Phys. J. C **33**, 75 (2004), hep-ph/0304107.
[24] G. Parisi, Phys. Rept. **103**, 203 (1984).
[25] G. P. Lepage, in *Theoretical Advanced Study Institute in Elementary Particle Physics* (1989).
[26] M. L. Wagman (2024), 2406.20009.
[27] D. C. Hackett and M. L. Wagman (2024), 2407.21777.
[28] D. C. Hackett and M. L. Wagman (2024), 2412.04444.
[29] L. Lellouch and M. Luscher, Commun. Math. Phys. **219**, 31 (2001), hep-lat/0003023.
[30] R. Abbott et al. (RBC, UKQCD), Phys. Rev. D **102**, 054509 (2020), 2004.09440.
[31] T. Blum et al. (RBC, UKQCD), Phys. Rev. D **104**, 114506 (2021), 2103.15131.
[32] N. Christ, X. Feng, J. Karpie, and T. Nguyen, Phys. Rev. D **106**, 014508 (2022), 2111.04668.
[33] T. Blum, P. A. Boyle, D. Hoying, T. Izubuchi, L. Jin, C. Jung, C. Kelly, C. Lehner, A. Soni, and M. Tomii (RBC, UKQCD), Phys. Rev. D **108**, 094517 (2023), 2306.06781.
[34] X. Gao, A. D. Hanlon, N. Karthik, S. Mukherjee, P. Petreczky, P. Scior, S. Shi, S. Syritsyn, Y. Zhao, and K. Zhou, Phys. Rev. D **106**, 114510 (2022), 2208.02297.
[35] A. Avkhadiev, P. E. Shanahan, M. L. Wagman, and Y. Zhao, Phys. Rev. Lett. **132**, 231901 (2024), 2402.06725.
[36] W. Detmold, A. V. Grebe, I. Kanamori, C. J. D. Lin, R. J. Perry, and Y. Zhao (HOPE), PoS **LATTICE2022**, 119 (2023), 2211.17009.
[37] D. Kovner, J. Karpie, K. Orginos, A. Radyushkin, and S. Zafeiropoulos (HadStruc), PoS **LATTICE2023**, 300 (2024), 2401.06858.
[38] R. G. Edwards, J. J. Dudek, D. G. Richards, and S. J. Wallace, Phys. Rev. D **84**, 074508 (2011), 1104.5152.
[39] J. Bulava, M. Donnellan, and R. Sommer, JHEP **01**, 140 (2012), 1108.3774.
[40] J. M. Zanotti, D. B. Leinweber, A. G. Williams, J. B. Zhang, W. Melnitchouk, and S. Choe (CSSM Lattice), Phys. Rev. D **68**, 054506 (2003), hep-lat/0304001.
[41] V. M. Braun, S. Collins, B. Gläßle, M. Göckeler, A. Schäfer, R. W. Schiel, W. Söldner, A. Sternbeck, and P. Wein, Phys. Rev. D **89**, 094511 (2014), 1403.4189.
[42] J. M. Zanotti, S. Choe, D. B. Leinweber, W. Melnitchouk, A. G. Williams, and J. B. Zhang, Nucl. Phys. B Proc. Suppl. **119**, 299 (2003), hep-lat/0210043.
[43] A. Bazavov et al. (MILC), Phys. Rev. D **87**, 054505 (2013), 1212.4768.
[44] K. Symanzik, Nucl. Phys. B **226**, 187 (1983).
[45] A. Hasenfratz and F. Knechtli, Phys. Rev. D **64**, 034504 (2001), hep-lat/0103029.
[46] B. Sheikholeslami and R. Wohlert, Nucl. Phys. B **259**, 572 (1985).
[47] R. J. Hudspith (RBC, UKQCD), Comput. Phys. Commun. **187**, 115 (2015), 1405.5812.
[48] M. A. Clark, R. Babich, K. Barros, R. C. Brower, and C. Rebbi (QUDA), Comput. Phys. Commun. **181**, 1517 (2010), 0911.3191.
[49] M. Gell-Mann and M. Levy, Nuovo Cim. **16**, 705 (1960).
[50] T. S. Evans and D. A. Steer, Nucl. Phys. B **474**, 481 (1996), hep-ph/9601268.
[51] M. Luscher, Commun. Math. Phys. **54**, 283 (1977).